Journal of Molecular Graphics and Modelling 54 (2014) 131–140

Contents lists available at ScienceDirect

Journal of Molecular Graphics and Modelling

journal homepage: www.elsevier.com/locate/JMGM

Reaction mechanism and free energy profile for acylation of Candida Antarctica lipase B with methylcaprylate and acetylcholine: Density functional theory calculations

Mohammad Sadegh Sadeghi Googheri [a,*], Mohammad Reza Housaindokht [a,b,**], Hassan Sabzyan [c]

[a] Biophysical chemistry laboratory, Department of Chemistry, Faculty of Science, Ferdowsi University of Mashhad, Mashhad, Iran
[b] Research and Technology Center of Biomolecules, Faculty of Science, Ferdowsi University of Mashhad, Mashhad, Iran
[c] Department of Chemistry, University of Isfahan, Isfahan, Iran

ARTICLE INFO

Article history:
Accepted 8 October 2014
Available online 22 October 2014

Keywords:
Enzyme-substrate interaction
MD simulation
QM investigation
Catalytic hydrolysis
Activation energy

ABSTRACT

Candida Antarctica lipase B (CALB), a specific enzyme to catalyze the hydrolysis of esters, can be a good candidate for acetylcholine (ACh) hydrolysis instead of acetylcholinesterase. The catalytic mechanism of the CALB acylation, as the first stage in the hydrolysis reaction, with ACh and methylcaprylate (MEC) has been examined by using density functional theory technique. The significant emphasis of this article is on the free energy barriers for the acylation step of hydrolysis reactions. Computed free energy barriers of the first step are 9.2 and 15.9 kcal mol^{-1}, but for the second step are 7.9 and 11.6 kcal mol^{-1} for MEC and ACh respectively. Activation free energies are in the comparable and acceptable range and imply both of two reactions are theoretically possible. The stability role of the adjacent amino acids was examined by using two applied tools. It is exposed that the oxyanion hole residues decrease energy barriers by stabilizing the transition state structures.

1. Introduction

The enzymatic reactions have an important role in the industrial, medicinal researches and human body. One of the most important enzymes, which is affected by different agents, is the acetylcholinesterase (AChE). Since AChE can hydrolyze the acetylcholine (ACh) and stops neurotransmission at cholinergic synapses, it is key enzyme in the nervous system of animals. In addition, AChE is a fast enzyme, especially for a serine hydrolase, functioning at a rate approaching that of a diffusion-controlled reaction.

Because of the importance of this enzyme, especially in the ACh hydrolysis reaction, it has been the subject of intensive investigations. AChE inhibitors are among the drugs that are approved by the FDA for management of Alzheimer's disease (AD). The powerful toxicity of organophosphorus (OP) poisons is attributed mostly to their activity as potent AChE inhibitors [1]. Although AChE has many advantages, it is not suitable for lab investigations because of its cost. Therefore, finding an economic and available enzyme with the same ability of AChE, especially the hydrolysis of ACh, is necessary. ACh is an ester of acetic acid and choline so the lipases, which are enzymes that have the ability to hydrolyse the ester compounds [2–4], can be candidate for this. One of the most often used lipases that have important applications in various industries is Candida Antarctica lipase B (CALB) that is an economic and common enzyme [5]. CALB belongs to the class of α/β-hydrolases, which all share a common protein structure characterized by mostly parallel β-sheets surrounded by α-helixes [6]. This enzyme has a catalytic triad consisting of three residues, aspartate, histidine and a nucleophilic serine. The serine residue is located at the nucleophilic elbow and the histidine is spatially at one side of the serine residue, where at the opposite side, a negative charge can be stabilized by a series of hydrogen bonds in the so-called oxyanion hole [7]. The CALB catalytic mechanism as AChE enzyme belongs to serine protease enzymes. Since the CALB active site and gorge structure as well as mechanism of action are like acetylcholinesterase, we decided to look at possibility of the acetylcholine hydrolysis by CALB. Here, the acylation step of hydrolysis reaction was investigated based on the reported catalytic mechanism [1,8–11]. The acylation step starts

* Corresponding author. Tel.: +98 0 511 8796505; fax: +98 0 511 8796416.
** Corresponding author at: Biophysical chemistry laboratory, Department of Chemistry, Faculty of Science, Ferdowsi University of Mashhad, Mashhad, Iran. Tel.: +98 0 511 8796505; fax: +98 0 511 8796416.
E-mail address: sadeghi.mohammadsadegh@gmail.com (M.S. Sadeghi Googheri).

http://dx.doi.org/10.1016/j.jmgm.2014.10.001
1093-3263/

with the enzyme-substrate complex formation by placing the substrate in the active site. Next, a nucleophilic attack is performed by the activated Serine to produce an unstable transition state (TS1). The tetrahedral intermediate (TI) that results from this unstable TS1, transforms to a steady state by passing through a transition state (TS2) and losing a methanol molecule. The product of this procedure is an acyl-enzyme (AE) complex that has an important role in these enzymatic reactions.

In this work, we employed density functional theory (DFT), which is the one of the quantum mechanics methods, to study the reaction pathway of the CALB acylation with ACh. Since the experimental results for the reaction between CALB and ACh did not exist, the reaction mechanism of CALB acylation with its experimental substrate, methylcaprylate (MEC), was examined and was used for comparison.

The tetrahedral intermediate (TI) structures were designed as the starting structures and other existent chemical species were created from it. We were using a two-step approach for reaction pathway analysis. At the first, optimization and frequency calculations of system were done at the low and executable computation level and then the single point calculations were performed at higher level to improve results.

Further, for better understanding of effective limits in the energy order of reaction pathway the natural bond orbital (NBO) [12] and atoms in molecules (AIM) [13] theories were used. With these useful tools, we can discuss the nature of existent interactions in the active site region and their effects on the configuration stability and energy barriers.

2. Materials and methods

2.1. Molecular dynamic simulation

Correct structures of the linked substrates and lipase B are required for the study of the acylation step of our interest. Therefore, the crystal structure of lipase B is taken from RCSB Protein Data Bank [14] (PDB ID: 1LBS [15]) and the linked inhibitor is converted to the MEC and ACh separately. To remove the steric of X-ray environment and considering the effects of aqueous solution on the enzyme structure, the 40 ns MD simulations was performed for these corrected structures on a Linux workstation by the Gromacs 4.5.4 software package [16] using the gromos force field. The initial structures of MEC and ACh were optimized by DFT calculations, at B3PW91/6-311++G(d, p) level of theory, and were used for creating the substrates force field parameters by the small-molecule topology generator PRODRG [17]. Afterward for modification of these substrate force fields their atomic charges were modified by the CHELPG procedure [18]. All systems were simulated in the isobaric–isothermal (NPT) ensemble at 300 K using periodic boundary conditions by using the Simple Point Charge (SPC) model [19] for water molecules. Weak coupling of the solutes to a constant temperature solvent bath were maintained using the Berendsen thermostat [20] with a coupling constant $\tau_T = 0.1$ ps. The pressure was controlled using the Parrinello-rahman algorithm [21] at one bar with a coupling constant $\tau_P = 2$ ps at 300 K. For all simulations, the neighbor list was updated every 10 steps, with a neighbor list cutoff distance of 1.2 nm. The long-range electrostatic interactions were modeled using the particle mesh Ewald (PME) summation method [22] with a cutoff distance of 1.2 nm for the real space. The integration time step is 2 fs, and the coordinates and velocities were saved every 4 ps. The LINCS algorithm [23] was used to restrain all bond lengths. Before the MD simulation, the system was energy minimized using 5000 steps of the steepest descent energy minimization method [24] to relax any created steric conflicts during the setup.

2.2. DFT calculations

Since the numbers of atoms in the enzyme-substrate complex is about 3000, the reaction pathway study by pure quantum computational methods is almost impossible. Therefore, a part of this complex involving the triad catalytic residue, oxyanion hole residues and the linked substrate in the active site region were selected by using the Arguslab software [25]. In these designed models, which were considered it as the tetrahedral intermediates (TIs) the QM subsystem has residues Ser105, His224, Asp187 as catalytic triad, residues Gln106 and Thr40 as the oxyanion hole region and connected substrates, ACh and MEC. DTF calculations were performed by applying the B3PW91 method in two steps for these two 108 and 111 atom structures, which are CALB-ACh and CALB-MEC respectively (Fig. 1).

The B3PW91 method uses two hybrid functional approximations, Becke three parameter [26] and Perdew-Wang91 [27], for estimation of the exchange–correlation energy functional. This offer an effective and exact method for calculation of non-local interactions as well as local interactions, which are efficient in the enzymatic reactions. In addition, this method has relatively good speed with respect to other improved methods that is lead to decrease the cost of computations.

In the first step, optimization was done at the best available and executable level of theory B3PW91/6-31G (d) followed by frequency calculations to confirm the nature of the stationary point [28–31]. Other chemical species containing enzyme-substrate (ES) and acyl-enzyme (AE) were created from this optimized construction and then optimization and frequency calculations of them were carried out at the same level of theory. Transition state structures, TS1 and TS2, were designed by gradually going from ES to TI and TI to AE respectively. The OPT = TS keyword was used for optimization of these unstable structures at the same level of theory. Please note that to keep the residues place in protein structure, the terminal atoms of them were frozen. To improve calculations of molecular geometries and properties, in second step, single point calculations were executed at B3PW91/6-311++G(d, p) [32] high-level of theory. The Conductor-like Polarizable Continuum Model (CPCM, solvent = water) was used for solvation effects [33,34]. All quantum mechanical calculations were performed by the Gaussian 09 [35] program packages.

Moreover, the NBO and AIM theories were used for quantitative investigation of the prophesied important interactions for different structures in these reaction pathways. The single point calculations in the solvent environment approach were used to gain the correct wave function files for AIM and NBO analyzes. All the QTAIM properties were calculated using the AIMQB program within the AIM Studio [36] suite, using the PROAIM basin integration method [37]. The NBO analyzes were carried out by using the NBO package included in Gaussian 09 suite of program [38].

3. Results and discussions

3.1. MD simulation results analysis

The first step of MD simulation analyses is a step to find out whether an equilibrium of the system was reached. For this purpose, the convergence of thermodynamic parameters such as temperature, potential and total energy of system is checked. In Fig. 2a the temperature of MD simulations of two enzyme-substrate systems are shown. As we can see, they change approximately between 295 K and 303 K so it has a very small deviation of the average value of 299.9 K. Since there is only a small fluctuation, the temperature in the system is quite stable and reaches an equilibrium. As we can see in Fig. 2b, the potential

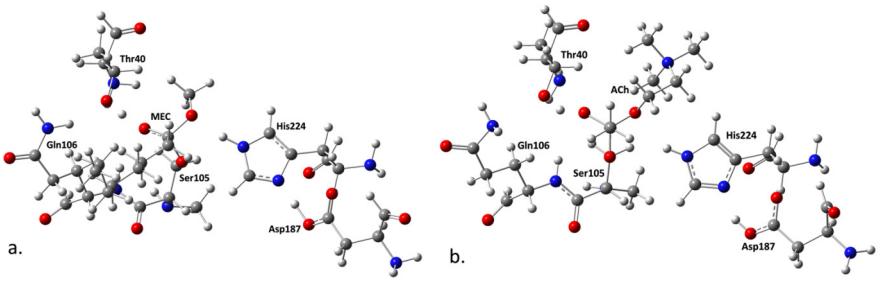

Fig. 1. The initial QM subsystems consist of 111 and 108 atoms for (a) CALB- MEC and (b) CALB-ACh.

energies of the simulated systems have the same behavior. They fluctuate in an approximate range of 5000 kJ mol^{-1}, which is very low compared to the average potential energies that are −5.33e + 05 and −4.97e + 05 kJ mol^{-1} for CALB-MEC and CALB-ACh systems respectively. This low potential fluctuation indicates that the protein is quite stable. Since the structure of a protein is responsible for the function of a protein, this stability is important for the function of the protein. By looking at Fig. 2c, we can see that

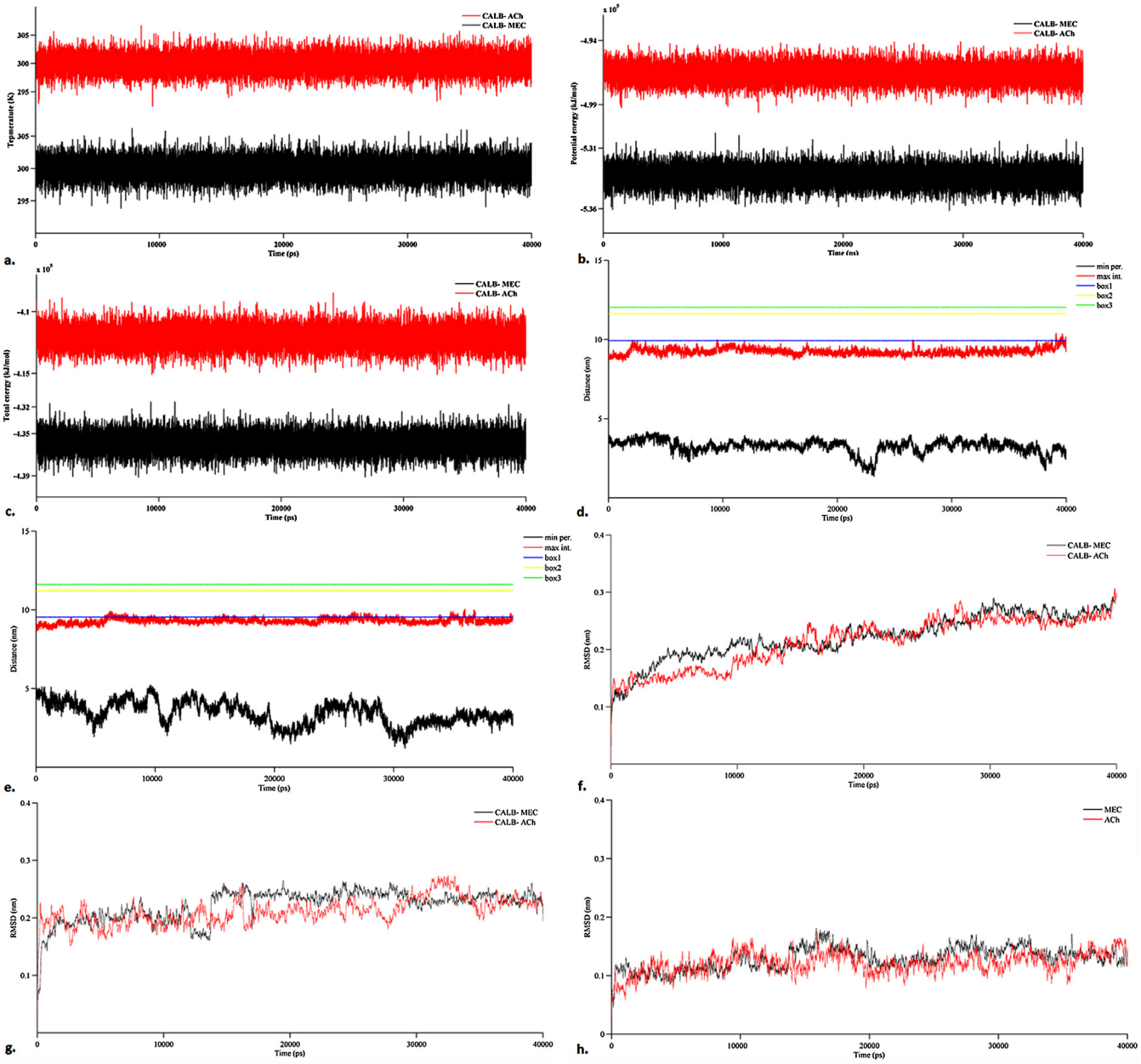

Fig. 2. The MD simulation analysis results. (a) Temperature, (b) potential and (c) total energy of enzyme-complexes during the simulation. (d) and (e) section of this figure show the minimum distance between periodic boundary cells for CALB-MEC and CALB-ACh complexes. RMSD of two structures for backbone, (f), active site, (g) and substrates, (h) are displayed.

there are less variation, approximately 4000 kJ mol^{-1}, in the total energies during the simulation, which stands for a stable protein and indicates that the simulations have reached equilibrium.

In the next step, we have to verify that there are no direct interactions between periodic images, as interactions between atoms of the same molecule over the periodic boundary would disturb the native behavior of the protein. Therefore, the minimum distance between periodic boundary cells was determined for two complex systems. Fig. 2d and e shows the distance variations during the simulation for two simulated systems. Data analysis indicates that the values range approximately between 1 and 5 nm. The shortest periodic distance for CALB-MEC is 1.332 nm at time 23,198 ps between atoms 24 and 2510 while it is 1.28 nm at time 30,944 ps between atoms 28 and 2628 for CALB-ACh complex. Both of these distances are more than the neighbor list cutoff distance, 1.2 nm, which confirms the quality of our MD simulations.

Furthermore, the conformational stability of enzyme-substrate complexes was investigated during the molecular dynamic simulation. For this purpose, the root mean square deviation (RMSD) from the initial structure throughout the simulation was examined. The overall RMSD, relative to minimized structures for two systems, which were computed on backbone atoms, active site residues and substrates, are shown in Fig. 2f, g and h respectively. As is clear after about 30,000 ps the backbone RMSD of two systems rise again a bit, so that the average value for the following time is about 0.25 nm. For the active site residue, they vary between 0.18 and 0.23 nm after 20,000 ps and converge approximately to 0.2 nm finally. A similar trend is observed for the RMSD of substrates with the final amount of 0.15 nm. All of the RMSD fluctuations indicate that the CALB-MEC and CALB-ACh complexes have stable conformation and the enzyme reactivity is retained.

Additionally we compared the equilibrated and minimized structures of our enzyme–substrate complexes in the active site region to show the structural changes during the simulation. In a and b sections of Fig. 3 show these structural fluctuations of the catalytic triad and oxyanion hole residues for CALB-MEC and CALB-ACh respectively. As can be seen these residues keep their critical positions through the MD simulations that leads to enzyme remains active. In c and d sections of this figure, most critical interactions between these residues and linked substrates after 40 ns simulations are shown. The expected hydrogen bonds in the active site region of two enzyme-substrate complexes are observable, which lead to stability and reactivity of them. The QM designed models of TIs, see Fig. 1, was created from these final snapshots of MD calculations.

3.2. Structural analysis of chemical species of reaction pathway

The catalytic pathway in which the CALB is acylated with MEC and ACh is presented in Fig. 4. As can be seen each acylation reaction has five chemical species including ES complex, two TS structures, one TI, and AE. The starting structures were TIs, which were optimized at B3PW91/6-31G (d) level of theory followed by frequency calculations. ES complexes and AE structures were created based on these initial constructions and were optimized at the same level of theory. No imaginary frequencies pointed out that we were in ground states, which are potential energy minimums in the potential energy surfaces (PES).

Based on a proposed mechanism the first step in this reaction pathway is the serine residue activation by the proton sharing in the catalytic triad, followed a nucleophilic attack on the carbonyl group of the substrate (Fig. 4). A stepwise approach is adopted for designing the transition states from ES structures. In this method, the carbonyl group of the substrate is transferred gradually to serine residue, and simultaneously, the serine residue proton is shifted to the Histidine residue. This procedure is carried out by scanning the relevant geometric structural coordinates (Fig. 5a).

From TI to AE, the tetrahedral intermediate undergoes a rearrangement toward a more stable structure by the transition structure TS2 shown in Fig. 4. As it can be seen from this figure, the carbon–oxygen double bond begins to form and simultaneously, the single bond between the same carbon atom and leaving group oxygen atom begins to break. The same technique as TS1 was used for scanning the pathway along these two coordinates to design TS2 structure, which their potential energy surfaces were displayed in Fig. 5b.

The maximums in the potential energy surfaces were chosen as the structures of transition states and were optimized to a transition state than a local minimum, using the Berny algorithm [39] at the same level of theory. Transition states were confirmed by imaginary frequencies in the vibrational frequency calculations.

The Enzyme-Substrate structure (ES): The acylation step starts with ES formation, which is molded by entering the substrate into the active site region and interacting with its residues. In the active site region the catalytic triad, which has an important role in these types of enzymatic reactions, is formed by proton sharing between Ser105, His224 and Asp187 residues. This significant triad can be deduced from structural analysis of optimized structures. Orientations of involved residues and their distances in our optimized constructions, see Figs. 6 and 7, imply hydrogen bonds (HBs) as the charge-relay network in catalytic triad.

Experimental investigations of the role of oxyanion hole in the substrate orientation in the active site are reported. The substrate interaction through oxygen atom of its carbonyl group with oxyanion hole may allow for insertion or positioning of a substrate, which would suffer from steric hindrance [40]. This role of oxyanion hole in the stabilizing is well represented in the optimized structures. The orientations of MEC and ACh substrates are such that the oxygen atom of carbonyl group forms the HB with Thr40 residue of oxyanion hole. It seems that the Gln106 residue, as another oxyanion hole residue, plays no role here (Figs. 6 and 7).

Above predictions about proton sharing and existence of HB network were a qualitative description so it was necessary that a quantitative judgment be performed for these structures. Therefore, for the first time the AIM and NBO computable tools were used for approval and interpretation of interactions in the active site region.

One of the powerful tools in analyzing the protons sharing is the NBO theory. HB formation notes that some of electronic charge is transferred from the proton acceptor to the proton donor and a rearrangement of electron density within each part of molecule has occurred. The power and place of the existing HBs can be determined by energies of these interactions, which is valued by the second order perturbation theory [41]. Significant donor–acceptor interactions and their second order perturbation energies in the catalytic triad and oxyanion hole areas of ES complexes are specified in Table 1.

As is obvious, the strong hydrogen bonding interactions in the active site region are caused energetic charge transfers between lone pairs (LP) and antibonds (σ^*) orbitals of donor and acceptor groups. In the catalytic triad the LP of Ser105 oxygen atom and nitrogen atom NO.2 of His224 act as donor NBO orbitals while σ^* of His224 N—H and Asp187 O—H bonds play the charge acceptor role. The same way is observed for oxyanion hole area, which the carbonyl oxygen atom of substrates puts its LP electrons at the σ^* of N—H and O—H bonds of Thr40 residue.

The AIM computable tool approves the existence of a bond critical point (BCP) between involved atoms, which the electron density (ρ) and Laplacian (∇^2_ρ) values of it decides the power and type of the

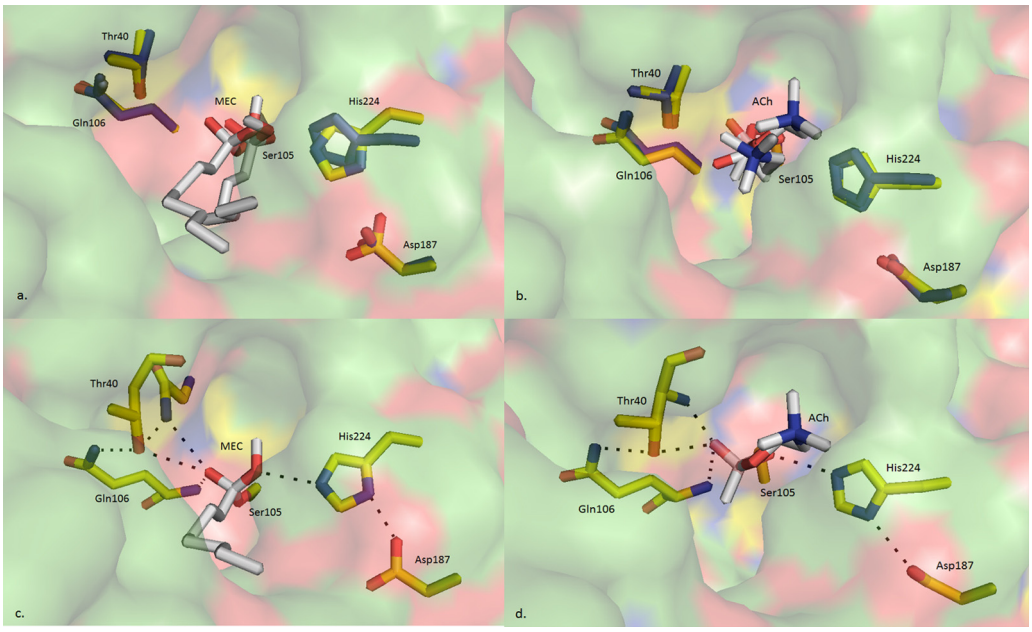

Fig. 3. Graphical comparison of equilibrated and minimized structures of our enzyme–substrate complexes in the active site region; (a) CALB-MEC and (b) CALB-ACh. The catalytic triad and oxyanion hole residues are presented as yellow and dark blue for after and before simulation respectively. The most important interactions between active site residue and substrates in the final snapshots of 40 ns MD simulations for CALB- MEC, (c), and CALB- ACh, (d). The substrates and involved residues are represented as sticks. Oxygen and nitrogen atoms are red and blue respectively. Carbon atoms of substrates are gray while of involved residues are shown as yellow. For better clearness, the hydrogen atoms are not shown. (For interpretation of the references to color in this figure legend, the reader is referred to the web version of the article.)

bond. For a localized covalent bond the ρ and ∇^2_ρ have positive and negative values while for a nonlocalized bond such as HB the ∇^2_ρ value is positive [42]. HB formation is associated with appearing a bond critical point between the hydrogen atom of donor group and acceptor atom [43]. To have a deeper knowledge about the possible HBs in ES complexes, a topological analysis of ρ_{BCP}, and its Laplacian, ∇^2_ρ were performed using AIM theory. Topological parameters (ρ, ∇^2_ρ) in all the bond critical point of ES complexes are given in Table 1. Matching to these results the formation bonds of catalytic triad include Ser105-O···HN-His224 and His224-N···HO-Asp187 while the C=O···HN-Thr40 and C=O···HO-Thr40 bonds are viewed in the oxyanion hole area. The watched ρ values vary between 0.014 and 0.070 whereas the ∇^2_ρ values of bond critical points find in the 0.055–0.154 a.u. These detected electron density properties

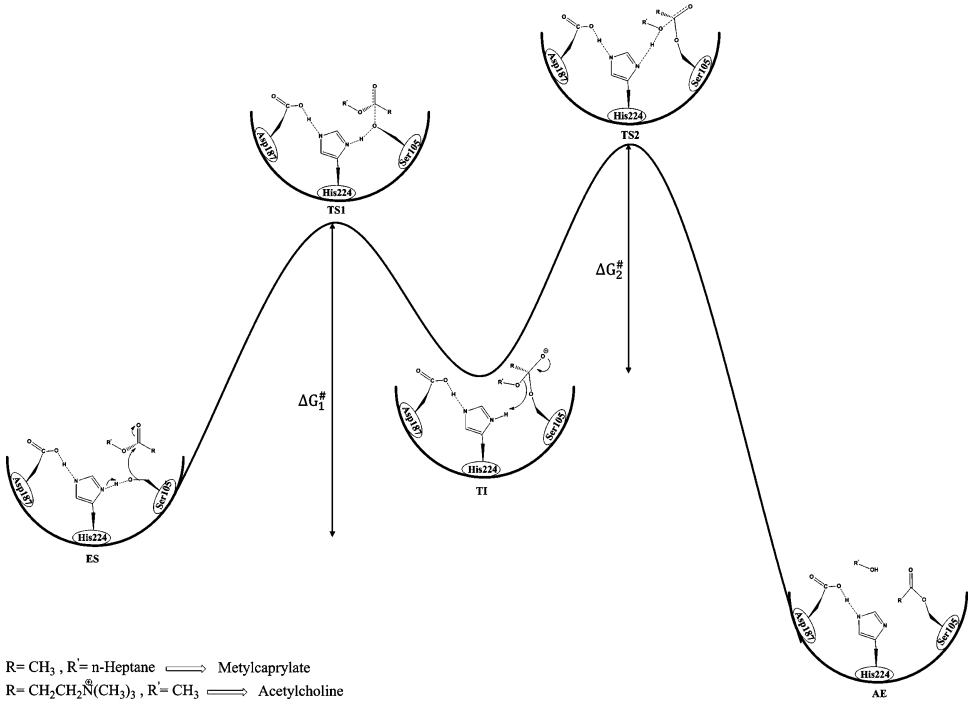

Fig. 4. Reaction pathway of CALB acylation including the five chemical species; enzyme-substrate (ES), tetrahedral intermediate (TI), transition states (TS1, TS2) and acyl-enzyme (AE).

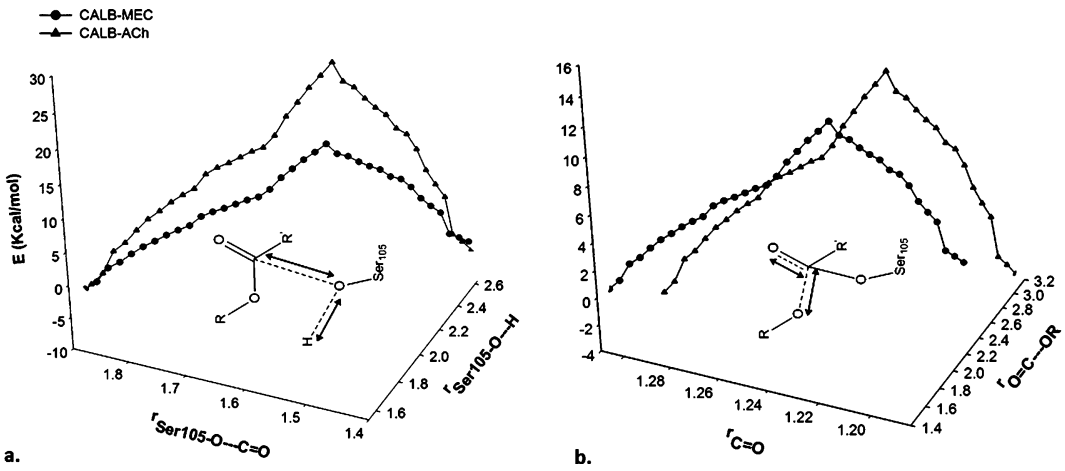

Fig. 5. Scanning scheme of passing from (a) TS1 and (b) TS2 for acylation steps of two reactions. The maximums in the potential energy surfaces were chosen as TS constructions. The scanned distances are in Å.

are as normal HB characters, which approve the hydrogen bonding interactions in the active site region.

Although both of ES complexes have proton sharing, but a noticeable difference can be observed between their strength from their electron density of bond critical points. The bond critical points in the catalytic triad and oxyanion hole have greater ρ values in the CALB-MEC complex than CALB-ACh, which implies the stronger HBs for it. This dissimilarity not only causes more stability of ES complex of CALB-MEC, but also increases its reactivity. Despite the steric hindrances, insertion of substrate in the active site area is simplified by stronger oxyanion hole HBs that leads to increase the stability of ES complex for CALB-MEC. Besides, the greater hydrogen bonding interactions in the catalytic triad increases the activity of Ser105 oxygen atom and speeds up the nucleophilic attack.

The first transition state structure (TS1): To go from ES complex to TI the reaction must pass through route TS1, see Fig. 4, which its optimized structures for acylation by MEC and ACh are shown in Figs. 6 and 7 respectively. Important differences between these two TS1 structures are seen from structural analysis. The distance between oxygen atom of Ser105 residue and carbonyl group of substrate, $r_{Ser105\text{-}O\cdots C=O}$, is longer while the Ser105-O···H

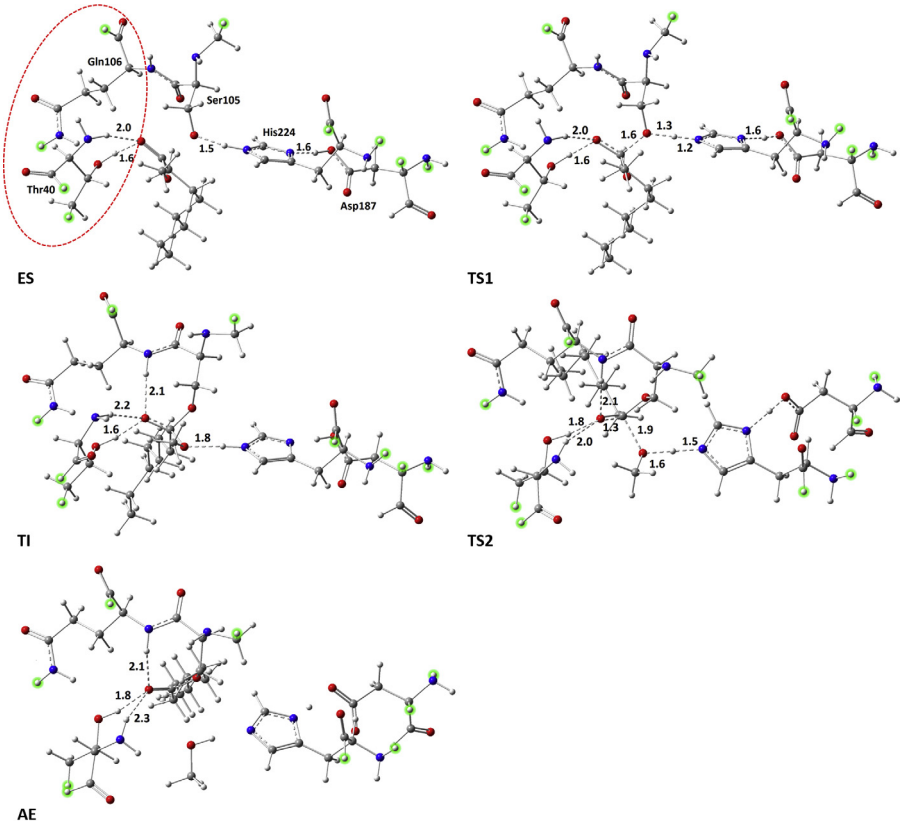

Fig. 6. Optimized structures of chemical species in the reaction pathway of CALB acylation with MEC substrate. Proposed HBs and their bond lengths, in Å, in the catalytic triad and oxyanion hole regions are shown. Fixed hydrogen atoms are displayed as green halos. The oxyanion hole residues, Gln106 and Thr40, are specified with red oval. (For interpretation of the references to color in this figure legend, the reader is referred to the web version of the article.)

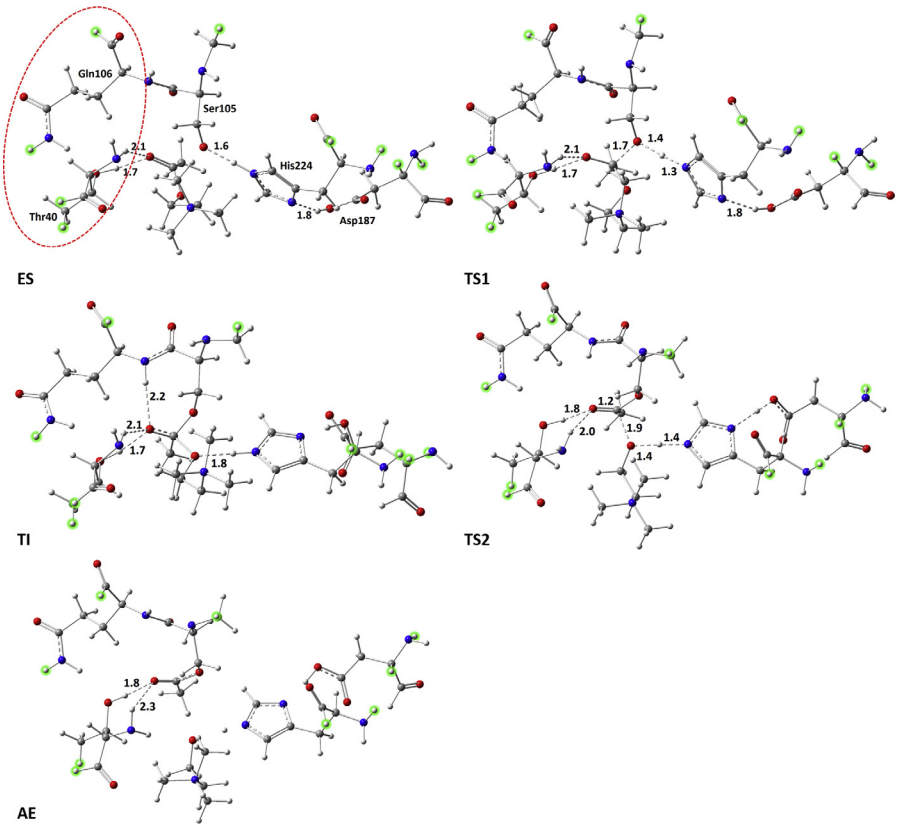

Fig. 7. Optimized structures of chemical species in the reaction pathway of CALB acylation with ACh substrate. Proposed HBs and their bond lengths, in Å, in the catalytic triad and oxyanion hole regions are shown. The oxyanion hole residues, Gln106 and Thr40, are specified with red oval. Fixed hydrogen atoms are displayed as green halos.

bond length is shorter for MEC than ACh. This means that in the acylation step by MEC the TS1 structure is formed with fewer displacements and reaching to the transition state is easier for this reaction. Also, the stronger HBs in the oxyanion hole region for MEC can be observed. More electron transfer energies and denser bond critical points, Table 1, imply stronger interactions for TS1 of MEC, which leads to greater stability for it. Therefore, we expect that the less energy is needed to pass from TS1 for acylation with MEC.

The tetrahedral intermediate structure (TI): as is mentioned when the nucleophilic attack of Ser105 residue occurs the ES complex by passing from TS1 structure converts to the stable tetrahedral intermediate. In this special structure, the side chain of Ser105 residue bonds to carbon atom of carbonyl group and carbon–oxygen double bond becomes single. This leads to formation a tetrahedral structure with a central carbon atom, which its oxygen atom carries a negative charge. This is where the role of oxyanion hole becomes more mentioned in this reaction by stabilizing this tetrahedral structure. Hydrogen bonding formation between the side chains of Thr40 and Gln106 residues with negative oxygen atom were distinguished from optimized structures. Calculated orientation of oxyanion hole residues with respect to

Table 1
Charge transfer energies and topological parameters of different chemical species of acylation reaction pathway. E (2) energies are in kcal mol-1 and ρ_{BCF} and its Laplacian are in a.u. Related figures of this table are exhibited in supporting information.

Chemical species	Involved NBO orbitals	$E^{(2)}$		ρ_{BCF}		∇_P^2	
		MEC	ACh	MEC	ACh	MEC	ACh
ES	$Lp_{C=O(sub)} \rightarrow \sigma^*_{O-H(Thr40)}$	32.8	25.8	0.058	0.048	0.154	0.148
	$Lp_{C=O(sub)} \rightarrow \sigma^*_{N-H(Thr40)}$	5.8	5.6	0.021	0.021	0.078	0.083
	$Lp_{O(Ser105)} \rightarrow \sigma^*_{N-H(His224)}$	41.9	37.8	0.070	0.062	0.153	0.149
	$Lp_{N(His224)} \rightarrow \sigma^*_{O-H(Asp187)}$	50.1	25.6	0.068	0.046	0.088	0.094
TS1	$Lp_{C=O(sub)} \rightarrow \sigma^*_{O-H(Thr40)}$	40.5	27.4	0.063	0.048	0.152	0.137
	$Lp_{C=O(sub)} \rightarrow \sigma^*_{N-H(Thr40)}$	6.2	5.5	0.021	0.018	0.078	0.075
	$Lp_{C=O(sub)} \rightarrow \sigma^*_{N-H(Gln106)}$	4.2	No	0.026	No	0.102	No
TI	$Lp_{C=O(sub)} \rightarrow \sigma^*_{O-H(Thr40)}$	32.6	26.4	0.053	0.047	0.138	0.132
	$Lp_{C=O(sub)} \rightarrow \sigma^*_{N-H(Thr40)}$	3.3	3.1	0.016	0.018	0.059	0.071
	$Lp_{C=O(sub)} \rightarrow \sigma^*_{N-H(Gln106)}$	7.0	5.8	0.019	0.018	0.059	0.055
	$Lp_{O(living\ group)} \rightarrow \sigma^*_{N-H(His224)}$	20.0	19.1	0.039	0.037	0.116	0.120
TS2	$Lp_{C=O(sub)} \rightarrow \sigma^*_{O-H(Thr40)}$	21.8	10.2	0.043	0.039	0.129	0.103
	$Lp_{C=O(sub)} \rightarrow \sigma^*_{N-H(Thr40)}$	2.2	1.3	0.015	0.011	0.098	0.062
	$Lp_{C=O(sub)} \rightarrow \sigma^*_{N-H(Gln106)}$	4.2	No	0.018	No	0.060	No

Table 2
Relative energies (ΔE), relative energies with zero-point energy corrections ($\Delta(E+ZPE)$) and relative Gibbs free energies (ΔG) in kcal mol^{-1}, of chemical species in the optimization, B3PW91/6-31G (d), and single point calculation, B3PW91/6-311++G (d, p), levels of theories in the water environment.

Chemical species	CALB-MEC				CALB-ACh			
	6-31G(d)		6-311++G(d,p)		6-31G(d)		6-311++G(d,p)	
	ΔE	$\Delta(E+ZPE)$	ΔG	ΔE	ΔE	$\Delta(E+ZPE)$	ΔG	ΔE
ES	0.0	0.0	0.0	0.0	0.0	0.0	0.0	0.0
TS1	10.3	9.7	9.2	8.3	16.9	15.6	15.9	14.6
TI	−7.2	−6.4	−6.8	−4.7	−1.2	−0.2	−1.7	−7.4
TS2	1.7	1.2	1.1	2.5	10.7	9.7	9.9	4.4
AE	−9.6	−10.0	−13.6	−15.6	−12.4	−12.9	−15.3	−10.2

tetrahedral structure, see Figs. 6 and 7, are in such a way that the HBs could be formed. These HBs form bond critical points between involved atoms which come from electron transfer between NBO orbitals (Table 1). Get involved of side chain of Gln106 residue in the HBs leads to stronger interactions in oxyanion hole for TI than ES complexes. Another special feature of TI construction was the leaving group orientation, which was obvious from structural analysis. This orientation is such that the oxygen atom of leaving group forms an HB with the side chain of His224 residue (Figs. 6 and 7 and Table 1). Because of this HB formation, the leaving ability of the products increases and going to AE becomes easier. This observation is consistent with the described results that confirm the HBs formation in this area and its critical role in the move toward the AE formation.

The second transition state structure (TS2): TS2 construction is formed in the pathway of TI to AE, which optimized structures for two reactions are shown in Figs. 6 and 7. To design the TS2 structures two parameters including the C—O bond length of carbonyl group, r_{C-O}, and the distance between carbon of carbonyl and oxygen of leaving groups, $r_{O-C\cdots OR}$, were scanned concurrently (Fig. 4b). Optimized bond length analysis shows that similar to TS1, this structure is made by less displacement for MEC. The bond lengths of r_{C-O} and $r_{O-C\cdots OR}$ are 1.3 and 1.8 for TS2 of MEC while they are 1.2 and 1.9 Å for ACh respectively (Figs. 6 and 7). In addition, stronger HBs in the oxyanion hole increase the stability of this structure for MEC (see Table 1).

The acyl-enzyme intermediate (AE): After passing through the TS2 state and removing the product of the acylation, the AE intermediate is formed. As is shown in Figs. 6 and 7, in this step the hydrogen of Serine is replaced by an acyl group, and methanol or choline molecule is released. This structure has an essential role in the enzyme reaction because if, instead of substrate, an inhibitor is located in the active site, the enzyme will be inhibited and the hydrolysis reaction stops. Inhibition of AChE by G-type and V-type agents comes from this fact [1,44].

3.3. Reaction pathway investigation

After predicting the individual structures of chemical species, the reaction pathway should be examined now. The energy values of the optimized structures of all species were extracted and the energies of the ES complexes were selected as the references for the comparative analysis of our interest. The relative energies are reported in Table 2, and the reaction pathways extracted of this are displayed in Fig. 8.

These results show that in the acylation step by MEC, 8.3–10.3 kcal mol^{-1} energy is required to pass over the energy barrier of TS1 while this energy is 14.6–16.9 kcal mol^{-1} for acylation

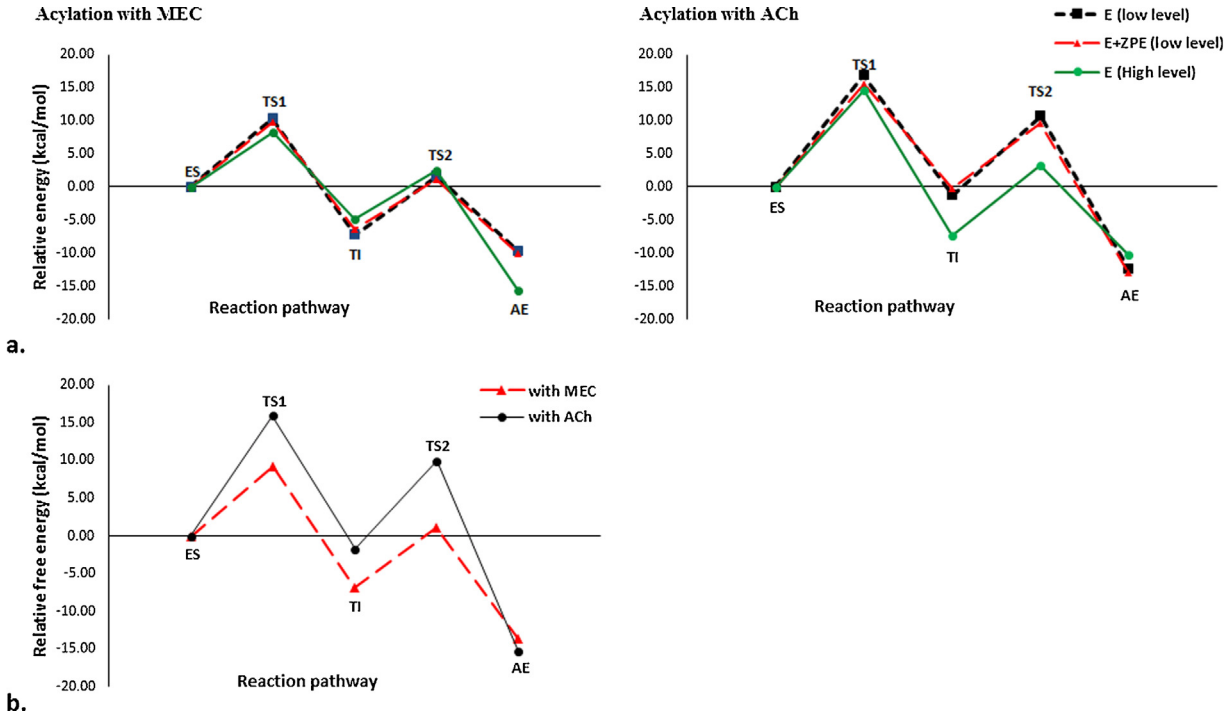

Fig. 8. (a) Reaction pathways of CALB acylation with MEC and ACh substrates based on energy viewpoint. The energy levels of chemical species are displayed for three types of calculations; low level, low level with put on zero-point correction and high level respectively. (b) Reaction pathways from Gibbs free energy lookout.

by ACh. Therefore, the energy barrier for acylation step with ACh is almost twice of MEC, which is consistent with our forecast from structural analysis. As was predicted the stronger HBs and weaker steric hindrance in the active site region of TS1 for MEC lead to more stability of TS1 structure and decrease the energy barrier for it.

Looks that the TI formation is with energy reducing such that in both reactions the energy of TI is lower than ES. This stable tetrahedral intermediate needs almost 7.2–8.9 kcal mol^{-1} of activation energy to cross over the TS2 energy barrier and convert to AE stable structure in the acylation with MEC. When the substrate becomes ACh, the energy barrier slightly increases and turns into nearly 9.9–11.9 kcal mol^{-1}. Likeness of energy barriers for this stage of reactions arises from the fact that both of reactions pass through the same path although the condition is a little better for acylation with MEC. As mentioned in this step of reaction the product of acylation step, methanol or choline, is produced and the AE structures is formed. Based on the earned results the AE construction is the most stable structure between all chemical species. Releasing of a stable molecule and decreasing of steric effects in the active site region lead to extra stability for this structure. This extraordinary stability shows the role of this step in the enzyme inhibition. If the acyl group forms a strong bond to the enzyme, the enzymatic reaction will be stopped in this step, and enzyme becomes inhibited.

In addition, the effect of the zero-point energy on the energy values of the optimization structures was examined. Zero-point energy correction does not affect on the stability order but it somewhat reduces the activation energies. The first activation energies become 9.7 and 15.6 kcal mol^{-1} for acylation with MEC and ACh while the second energy barriers be converted into 7.6 and 9.9 kcal mol^{-1} for these reactions respectively (Table 2). These energy barriers are closer to calculated values from high-level calculations than uncorrected energies. These mark hereby that applying zero-point energy correction the better results can be gained without increasing the cost of calculations.

So the relative Gibbs free energies of acylation step for two reactions, which are gained by using the frequency calculations in the low-level of theory, can be used for pathway investigation from the free energy viewpoint (Fig. 8b). As is obvious the changes trend of free energies are similar to relative energy changes with a little decrease in activation energy values. The first and second free energy barrier are reduced almost as much as 1 kcal mol^{-1} for two reactions. Although the ACh substrate wants twice free energy to cross over TS1 than MEC, but it is in the acceptable range of activation energy. This value of free energy is comparable with energies that were reported for the acylation step of AChE and BuChE hydrolysis with ACh. In the computational studies that were done by Yanzi Zhou [45] and Xi Chen [46] the calculated free energy barriers for passing from first transition states are almost between 12.3 and 13.4 kcal mol^{-1}. Based on this observation we can say that although the ACh needs more energy than MEC for the reaction and cannot compete with MEC, but it can theoretically acylate the CALB enzyme.

4. Conclusion

The reaction pathway of the acylation step of methylcaprylate and acetylcholine hydrolysis reactions by lipase B was studied by DFT methods starting from a Ping-Pong bi-bi mechanism was suggested before. Five different species including the enzyme-substrate complex, transition states, tetrahedral intermediate and acyl-enzyme structure along the two reaction paths were identified and examined by two levels of theories. Structures optimization in the water environment was performed in the lower level of theory, B3PW91/6-31G (d), following by frequency calculations and the single point computations on the optimized structures were carried out by applying the large basis sets, 6-311++G (d, p), in the same method. The density of bond critical point and electron transfer energies explored the type and strength of interactions in the active site region, which were reached by using AIM and NBO tools.

Calculated energy barriers of two reactions were reported for optimization and single point calculations. For the acylation with MEC, the first activation energy was 10.3 kcal mol^{-1} in the optimization level that with put on zero-point energy correction was converted to 9.7 kcal mol^{-1}. This value of energy reduced to 8.3 kcal mol^{-1} with enlarging the basis sets. The same procedure was viewed for second energy barrier, which the energy barriers changed from 8.89 to 7.2 kcal mol^{-1}. Acylation reaction with ACh was going through a similar process with twice energy values such that activation energies, with consideration of mentioned corrections, transformed from 16.9 to 14.6 and 11.9 to 9.9 kcal mol^{-1} for the first and second steps respectively.

In addition, the reaction pathways were surveyed from the Gibbs free energy viewpoint. From this perspective, when the substrate was MEC the CALB was acylated with 9.7 and 7.9 kcal mol^{-1} of activation free energies for the first and second steps respectively. While the CALB acylation with ACh had occurred with 15.9 for the first and 11.6 kcal mol^{-1} for the second free energy barriers. According to the minimized energy profile for acylation by ACh and comparison with the available data reported for similar reactions, the reaction pathway, its transition states and intermediates is approved and suggested that this reaction may be theoretically possible.

Acknowledgments

This research was supported by Ferdowsi University of Mashhad, Iran (grant 3/20408-07 March 2012).

Appendix A. Supporting information.

The NBO and AIM structures of all chemical species can be found in supporting information data.

Appendix B. Supplementary data

Supplementary data associated with this article can be found, in the online version, at http://dx.doi.org/10.1016/j.jmgm.2014.10.001.

References

[1] K. Kim, O.G. Tsay, D.A. Atwood, D.G. Churchill, Destruction and detection of chemical warfare agents, Chem. Rev. 111 (2011) 5345–5403.
[2] G.D. Yadav, K.M. Devi, Enzymatic synthesis of perlauric acid using Novozym 435, Biochem. Eng. J. 10 (2002) 93–101.
[3] I. Mathews, M. Soltis, M. Saldajeno, G. Ganshaw, R. Sala, W. Weyler, et al., Structure of a novel enzyme that catalyzes acyl transfer to alcohols in aqueous conditions, Biochemistry 46 (2007) 8969–8979.
[4] F. Björkling, H. Frykman, S.E. Godtfredsen, O. Kirk, Lipase catalyzed synthesis of peroxycarboxylic acids and lipase mediated oxidations, Tetrahedron 48 (1992) 4587–4592.
[5] M. Martinelle, M. Holmquist, K. Hult, On the interfacial activation of Candida Antarctica lipase A and B as compared with Humicola lanuginosa lipase, Biochim. Biophys. Acta Lipids Lipid Metab. 1258 (1995) 272–276.
[6] M. Nardini, B.W. Dijkstra, α/β hydrolase fold enzymes: the family keeps growing, Curr. Opin. Struct. Biol. 9 (1999) 732–737.
[7] Z.S. Derewenda, A.M. Sharp, News from the interface: the molecular structures of triacyglyceride lipases, Trends Biochem. Sci. 18 (1993) 20–25.
[8] C. Li, T. Tan, H. Zhang, W. Feng, Analysis of the conformational stability and activity of Candida Antarctica lipase B in organic solvents, J. Biol. Chem. 285 (2010) 28434–28441.
[9] A. Houde, A. Kademi, D. Leblanc, Lipases and their industrial applications: an overview, Appl. Biochem. Biotechnol. 118 (2004) 155–170.
[10] M. Martinelle, K. Hult, Kinetics of acyl transfer reactions in organic media catalysed by Candida Antarctica lipase B, Biochim. Biophys. Acta 1251 (1995) 191–197.
[11] J. Kraut, Serine proteases: structure and mechanism of catalysis, Annu. Rev. Biochem. 46 (1977) 331–358.
[12] A.E. Reed, R.B. Weinstock, F. Weinhold, Natural population analysis, J. Chem. Phys. 83 (1985) 735–746.

[13] R.F.W. Bader, Atoms in Molecules: A Quantum Theory, Oxford University Press, Incorporated, 1994.
[14] H.M. Berman, J. Westbrook, Z. Feng, G. Gilliland, T.N. Bhat, H. Weissig, et al., The Protein Data Bank, Nucleic Acids Res. 28 (2000) 235–242.
[15] J. Uppenberg, N. Ohrner, M. Norin, K. Hult, G.J. Kleywegt, S. Patkar, et al., Crystallographic and molecular-modeling studies of lipase B from Candida Antarctica reveal a stereospecificity pocket for secondary alcohols, Biochemistry 34 (1995) 16838–16851.
[16] B. Hess, C. Kutzner, D. van der Spoel, E. Lindahl, GROMACS 4 algorithms for highly efficient load-balanced, and scalable molecular simulation, J. Chem. Theory Comput. 4 (2008) 435–447.
[17] A.W. Schuttelkopf, D.M. van Aalten, PRODRG: a tool for high-throughput crystallography of protein–ligand complexes, Acta Crystallogr. D: Biol. Crystallogr. 60 (2004) 1355–1363.
[18] C.M. Breneman, K.B. Wiberg, Determining atom-centered monopoles from molecular electrostatic potentials the need for high sampling density in formamide conformational analysis, J. Comput. Chem. 11 (1990) 361–373.
[19] G.W. Robinson, Water in Biology, Chemistry, and Physics: Experimental Overviews and Computational Methodologies, World Scientific, Singapore, River Edge, 1996.
[20] H.J.C. Berendsen, J.P.M. Postma, W.F. van Gunsteren, A. DiNola, J.R. Haak, Molecular dynamics with coupling to an external bath, J. Chem. Phys. 81 (1984) 3684–3690.
[21] M. Parrinello, A. Rahman, Polymorphic transitions in single crystals: a new molecular dynamics method, J. Appl. Phys. 52 (1981) 7182–7190.
[22] T. Darden, D. York, L. Pedersen, Particle mesh Ewald: An N [center-dot] log(N) method for Ewald sums in large systems, J. Chem. Phys. 98 (1993) 10089–10092.
[23] B. Hess, H. Bekker, H.J.C. Berendsen, J. Fraaije, LINCS: a linear constraint solver for molecular simulations, J. Comput. Chem. 18 (1997) 1463–1472.
[24] M.C. Payne, M.P. Teter, D.C. Allan, T.A. Arias, J.D. Joannopoulos, Iterative minimization techniques for ab initio total-energy calculations: molecular dynamics and conjugate gradients, Rev. Mod. Phys. 64 (1992) 1045–1097.
[25] M.A. Thompson, Molecular docking using ArgusLab, an efficient shape-based search algorithm and the AScore scoring function, in: ACS Meeting, Philadelphia, PA, 172, 2004, CINF 42.
[26] A.D. Becke, Density functional thermochemistry III. The role of exact exchange, J. Chem. Phys. 98 (1993) 5648–5652.
[27] P. Ziesche, H. Eschrig, Technische Universitat Dresden. Institut fur Theoretische Physik, European Physical Society, Electronic Structure of Solids '91: Proceedings of the 75. WE-Heraeus-Seminar and 21st Annual International Symposium on Electronic Structure of Solids held in Gaussig (Germany), Akademie Verlag, Berlin, Germany, 1991, March.
[28] D.B. Axel, A new mixing of Hartree–Fock and local density-functional theories, J. Chem. Phys. 98 (1993) 1372.
[29] C. Lee, W. Yang, R.G. Parr, Development of the Colle–Salvetti correlation-energy formula into a functional of the electron density, Phys. Rev. B. 37 (1988) 785–789.
[30] S.H. Vosko, L. Wilk, M. Nusair, Accurate spin-dependent electron liquid correlation energies for local spin density calculations: a critical analysis, Can. J. Phys. 58 (1980) 1200–1211.
[31] P.J. Stephens, F.J. Devlin, C.F. Chabalowski, M.J. Frisch, Ab initio calculation of vibrational absorption and circular dichroism spectra using density functional force fields, J. Phys. Chem. 98 (1994) 11623–11627.
[32] A.K. Rappe, C.J. Casewit, K.S. Colwell, W.A. Goddard, W.M. Skiff, UFF, a full periodic table force field for molecular mechanics and molecular dynamics simulations, J. Am. Chem. Soc. 114 (1992) 10024–10035.
[33] V. Barone, M. Cossi, Quantum calculation of molecular energies and energy gradients in solution by a conductor solvent model, J. Phys. Chem. A 102 (1998) 1995–2001.
[34] M. Cossi, N. Rega, G. Scalmani, V. Barone, Energies, structures, and electronic properties of molecules in solution with the C-PCM solvation model, J. Comput. Chem. 24 (2003) 669–681.
[35] M.J. Frisch, G.W. Trucks, H.B. Schlegel, G.E. Scuseria, M.A. Robb, J.R. Cheeseman, et al., Gaussian 09, Revision B.01, Wallingford, CT, 2009.
[36] T. Keith, AIMAll 10.05.04. TK Gristmill Software, 2010.
[37] S. Jenkins, Z. Liu, S.R. Kirk, A bond, ring and cage resolved Poincaré–Hopf relationship for isomerisation reaction pathways, Mol. Phys. 111 (2013) 3104–3116.
[38] Glendening, E.D., Reed, A.E., Carpenter, J.E., Weinhold, F. NBO Version 3.1 (1998).
[39] C. Peng, P.Y. Ayala, H.B. Schlegel, M.J. Frisch, Using redundant internal coordinates to optimize equilibrium geometries and transition states, J. Comput. Chem. 17 (1996) 49–56.
[40] D.L. Nelson, A.L. Lehninger, M.M. Cox, Lehninger Principles of Biochemistry, W. H. Freeman, New York, USA, 2008.
[41] A. Nowroozi, H. Roohi, M.S. Sadeghi Ghoogheri, M. Sheibaninia, The competition between the intramolecular hydrogen bond and (-electron delocalization in trifluoroacetylacetone—a theoretical study, Int. J. Quantum Chem. 111 (2011) 578–585.
[42] M.R. Housaindokht, H.E. Hosseini, M.S. Sadeghi Googheri, H. Monhemi, R.I. Najafabadi, N. Ashraf, et al., Hydrogen bonding investigation in 1-ethyl-3-methylimidazolium based ionic liquids from density functional theory and atoms-in-molecules methods, J. Mol. Liquids 177 (2013) 94–101.
[43] A. Nowroozi, A.F. Jalbout, H. Roohi, E. Khalilinia, M. Sadeghi, A. de Leon, et al., Hydrogen bonding in acetylacetaldehyde: theoretical insights from the theory of atoms in molecules, Int. J. Quantum Chem. 109 (2009) 1505–1514.
[44] R.T. Delfino, T.S. Ribeiro, J.D. Figueroa-Villar, Organophosphorus compounds as chemical warfare agents: a review, J. Braz. Chem. Soc. 20 (2009) 407–428.
[45] Y. Zhou, S. Wang, Y. Zhang, Catalytic reaction mechanism of acetylcholinesterase determined by born-oppenheimer ab initio QM/MM molecular dynamics simulations, J. Phys. Chem. B 114 (2010) 8817–8825.
[46] X. Chen, L. Fang, J. Liu, C.-G. Zhan, Reaction pathway and free energy profile for butyrylcholinesterase-catalyzed hydrolysis of acetylcholine, J. Phys. Chem. B 115 (2010) 1315–1322.